Structural Engineering and Mechanics, Vol. 41, No. 5 (2012) 645-662

DOI: http://dx.doi.org/10.12989/sem.2012.41.5.645

Simulation of corroded RC structures using a three-dimensional irregular lattice model

Kunhwi Kim[1a], John E. Bolander[2b] and Yun Mook Lim[1*]

[1]Department of Civil & Environmental Engineering, Yonsei University, Seoul, Korea
[2]Department of Civil & Environmental Engineering, University of California, Davis, USA

(Received September 22, 2011, Revised January 9, 2012, Accepted February 2, 2012)

Abstract. Deteriorative effects of steel corrosion on the structural response of reinforced concrete are simulated for varying degrees of corrosion. The simulation approach is based on a three-dimensional irregular lattice model of the bulk concrete, in which fracture is modeled using a crack band approach that conserves fracture energy. Frame elements and bond link elements represent the reinforcing steel and its interface with the concrete, respectively. Polylinear stress-slip properties of the link elements are determined, for several degrees of corrosion, through comparisons with direct pullout tests reported in the literature. The link properties are then used for the lattice modeling of reinforced concrete beams with similar degrees of corrosion of the main reinforcing steel. The model is successful in simulating several important effects of steel corrosion, including increased deflections, changes in flexural cracking behavior, and reduced yield load of the beam specimens.

Keywords: steel corrosion; reinforced concrete; irregular lattice model; concrete-reinforcement interface; fracture

1. Introduction

Corrosion of reinforcing steel is one of the major problems facing reinforced concrete (RC) structures exposed to severe environments. Corrosion leads to loss of bar cross section, possible cracking/spalling of the concrete cover, and changes in bonding properties. In addition to strength issues, bond performance affects lateral deflection and maximum crack width, which are serviceability criteria within the limit state design of beams. Several experimental programs have studied the potential reductions in the strength of RC members due to steel corrosion (Al-sulaimani *et al.* 1990, Lee 1997). Results from the studies indicate that corrosion effects can play a dominant role in determining the failure mode of the structural component and/or system (Lee 1997). Despite these observations, however, the effects of corrosion or other deterioration of bonding are largely neglected in conventional structural engineering practice.

The bond of deformed steel bars generally has two components: chemical adhesion between the steel and concrete; and mechanical interlocking due to the bar lugs bearing against the concrete.

*Corresponding author, Professor, E-mail: yunmook@yonsei.ac.kr
[a]Research Scholar, E-mail: kunhwi@yonsei.ac.kr
[b]Professor, E-mail: jebolander@ucdavis.edu

Experimental programs have demonstrated the importance of various parameters affecting bond, including bar size and lug geometry, concrete strength, embedment length, degree of confinement, and loading type (Stanish *et al.* 1999). Common tests, which can be broadly classified into pullout tests and flexural tests, have shown that average bond strength generally decreases with increases in the embedment length and bar diameter (Mathey and Watstein 1961). The large majority of bond tests have been for bars without significant degrees of corrosion.

The degree to which corrosion related damage affects structural performance needs further study through laboratory testing, monitoring of field performance, and numerical modeling. Validated numerical models are useful for interpreting lab and field work, and enable investigations outside of the parameter ranges covered by physical testing. Time dependency of corrosion processes and the potentially large scales of actual structures make laboratory testing difficult. Furthermore, modeling provides a direct means for associating degradation of local bond properties and loss of bar cross-section area to overall structural performance.

The modeling of reinforcing steel corrosion and its effects has generally concerned either:

1. the time-dependent processes of corrosion and cracking local to individual bars. Corrosion is often conceptualized as a two-phase process consisting of an initiation phase, in which some protective barrier is being overcome, and a propagation phase involving active corrosion (Tuutti 1982). The modeling of corrosion and bond actions local to the bar surface enables more physically-based simulations of pullout and/or splitting failure due to corrosion (Bažant 1979, Cairns and Abdullah 1996, Coronelli 2002, Hansen and Saouma 1999, Liu and Weyers 1998, Pantazopoulou and Papoulia 2001); or
2. understanding the effects of bond deterioration on structural performance (Stanish *et al.* 1999). For this purpose, the modeling of bond usually needs to be simplified. For example, the various components of bond and their degradation have been modeled using bond stress versus slip relations, and the time-dependency of the corrosion process is prescribed using basic equations. Such macroscopic modeling of bond has been the most common approach for finite element analysis of RC structures (Task Committee on Finite Element Analysis of Reinforced Concrete Structures 1982). Typical bond stress-slip relationships have been provided by the experimental and analytical work of Ciampi *et al.* (1982) and Eligehausen *et al.* (1983). Abrishami and Mitchell examined the combination of pull-out and push-in tests to control the bond stress distribution (Abrishami and Mitchell 1992), and then developed an analytical approach for predicting the responses of both pull-out failures and splitting failures (Abrishami and Mitchell 1996).

In this paper, the second of the two modeling objectives has been pursued: a three-dimensional lattice model is used to study the effects of reinforcing steel bond deterioration on strength, lateral deflections, and cracking patterns of RC beams. The lattice model consists of a Rigid-Body-Spring Network representing the concrete continuum, frame elements representing the reinforcing bars, and bond link elements representing the macroscopic properties of the steel-concrete interface (Bolander *et al.* 2000, Bolander and Saito 1998). The macro-modeling of bond is based on a polylinear representations of the bond stress-slip curve, which are determined through comparisons with concentric pullout test results (obtained from the literature) for differing degrees of corrosion. The calibrated bond link elements are then used in forward analyses of laterally-loaded RC beams tested by Lee (1997). Note that uniform corrosion and the corresponding deterioration effects are considered for the modeling objective of this study. Comparisons of the numerical and physical experiments help validate the proposed modeling approach, and also provide insight into some practical implications of bond deterioration in RC structures.

2. Lattice model of structural concrete

Structural concrete is modeled as a three-component system consisting of concrete, reinforcing steel bars, and the concrete-steel interface. Each component is represented by simple, two-node elements, as described in the following sections. The overall collection of elements is best categorized as an irregular lattice model.

2.1 Concrete

The volume of concrete is assumed to be homogeneous and is discretized using an irregular lattice of rigid-body-spring elements, as shown in Figs. 1 and 2. Discretization begins with the placement of nodes in the domain using a process of sequential random addition (Widom 1966), in which the minimum allowable distance between any two nodes is prescribed. The lattice topology is defined by the Delaunay tessellation (Preparata and Shamos 1985) of this set of nodal points; rendering of the concrete volume, and the assignment of lattice element properties, is based on the dual Voronoi tessellation of the same set of nodes. Voronoi tessellations have qualities that are of increasing interest within the general field of solid mechanics (Sukumar and Bolander 2008).

A lattice element is defined by two natural neighbors, nodes i and j, and their common Voronoi facet (Fig. 2). Element stiffness formulations are based on the rigid-body-spring concept of Kawai (1978). The two nodes are connected via rigid-body constraints and a zero-size spring set located at the centroid C of the Voronoi facet. In this three-dimensional setting, each node has six degrees of freedom. The spring set is composed of three axial springs, aligned with normal and tangential directions $n-s-t$ as shown in Fig. 2, and three rotational springs (not depicted in the figure) about the same axes. The stiffness coefficients of the axial springs are

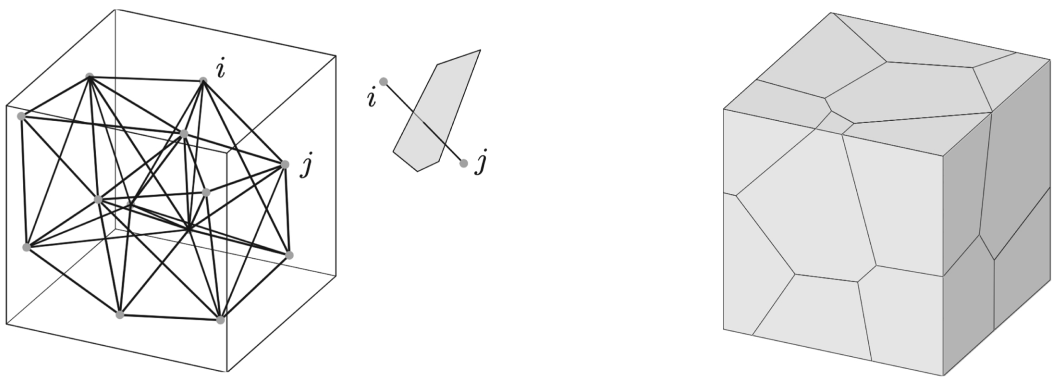

(a) (b)

Fig. 1 Structural domain discretization; (a) Lattice topology defined by the Delaunay tessellation of semi-random point set (with a view of element ij extracted from the lattice), (b) Volume rendering based on the dual Voronoi tessellation of the point set

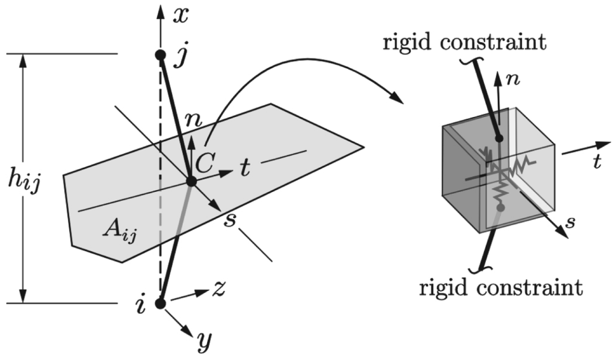

Fig. 2 Lattice element *ij* and view of zero-size spring set positioned at point *C*

$$k_n = \alpha_1 E \frac{A_{ij}}{h_{ij}} \tag{1}$$

and

$$k_s = k_t = \alpha_2 k_n \tag{2}$$

where A_{ij} is the area of the common Vornoi facet; h_{ij} is the Euclidean distance between the element nodes; and factors α_1 and α_2 are adjusted (via uniaxial load test simulation) to provide global representation of both Young's modulus E and Poisson ratio ν. For the special case where α_1 and α_2 are set to unity, the lattice network provides an exact, elastically homogenous representation of E, although the corresponding value $\nu = 0$ (Bolander and Saito 1998, Yip *et al.* 2005). Assignment of the stiffness coefficients for the rotational springs $(k_{\phi n}, k_{\phi s}, k_{\phi t})$ is based on the sectional properties of A_{ij} and the element length h_{ij}, as described elsewhere (Yip *et al.* 2005).

The element stiffness matrix is

$$\mathbf{k} = \mathbf{T}^T(\mathbf{B}^T\mathbf{D}\mathbf{B})\mathbf{T} \tag{3}$$

where **B** is a matrix relating element nodal and spring set local displacements (Kawai 1978, Yip *et al.* 2005) and **T** is the transformation matrix relating element-local and global coordinate systems (McGuire and Gallagher 1979). Element stiffness matrices are assembled into the system stiffness matrix **K** in a conventional manner (Hughes 1987). **D** is the material matrix defined by

$$\mathbf{D} = (1-\omega)\mathrm{diag}[k_n, k_s, k_t, k_{\phi n}, k_{\phi s}, k_{\phi t}] \tag{4}$$

where ω is a scalar measure of damage used, in conjunction with a crack band model (Bažant and Oh 1983), to represent concrete fracture. The crack band forms perpendicular to the direction of principal tension, as determined by the resultant of axial spring forces $F_R = (F_n^2 + F_s^2 + F_t^2)^{1/2}$. The dimensions of the crack band are constrained to the local geometry of the Voronoi diagram, as shown for planar elements in Fig. 3(a). The fracture criterion is founded on a measure of normal stress, according to

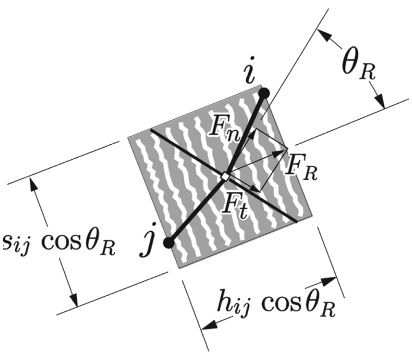

(a)

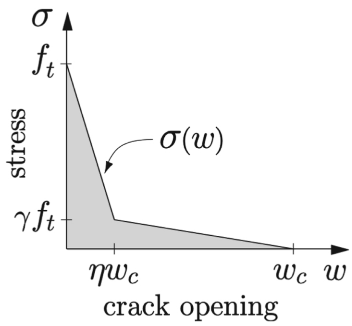

(b)

Fig. 3 Crack band model of concrete fracture; (a) implementation of crack band concept within planar lattice element *ij*, (b) softening diagram

$$\sigma_R = \frac{F_R}{A_{ij}^P} \tag{5}$$

in which A_{ij}^P is the projection of A_{ij} in the direction of F_R. For the planar analysis case shown in Fig. 3(a), $A_{ij}^P = s_{ij}\cos\theta_R b$, where s_{ij} is the length of the Voronoi segment shared by nodes i and j; and b is the thickness of the element. The relationship between normal stress and crack opening displacement is assumed to be a bilinear function (Fig. 3(b)). The crack band implementation within the lattice provides a grid insensitive, energy conserving representation of fracture for both two- and three-dimensional analyses (Berton and Bolander 2006, Bolander and Sukumar 2005). Concrete material non-linearity for other stress conditions, including compression, has been implemented in a planar version of this lattice approach (Bolander *et al.* 2000), but has not been considered here. For the under-reinforced concrete beams studied later, modeling of tensile cracking is sufficient for studying early crack development and behavior just beyond yield of the reinforcing steel, which are the foci of the comparisons made for differing degrees of steel corrosion.

2.2 Reinforcement

The trajectory of the reinforcement is prescribed independently from the geometry of the lattice. The trajectory can be curvilinear, in which case the reinforcement is divided into a series of linear segments, i.e., 1-D line elements. With sufficient mesh resolution, curved reinforcement profiles can be accurately represented (Yip *et al.* 2005).

Fig. 4(a) shows a typical segment of reinforcement as it passes through the Voronoi cells associated with several concrete nodes. The reinforcement is represented as a series of ordinary 3-D frame elements (McGuire and Gallagher 1979); the frame element nodes are automatically positioned on the mid-point along the path within each Voronoi cell through which the reinforcement passes (e.g., frame element node I is placed midway along segment $\overline{qr}$ in Fig. 4(b)).

The axial component of the frame elements accounts for linear elastic, linear strain-hardening behavior, as shown in Fig. 5 where E_s is the modulus of elasticity of the steel and β is the post-yield hardening coefficient. With respect to flexure and torsion, the frame elements are linear elastic. For the cases where bar corrosion occurs, the reduced cross-sectional area of the bar is

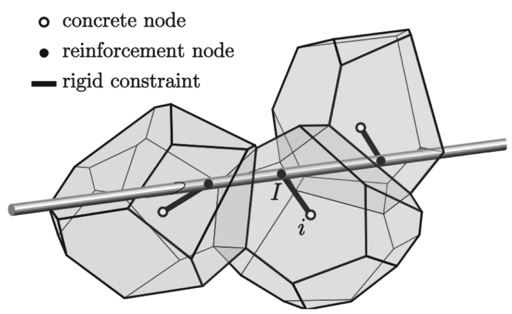

(a) Link element iI

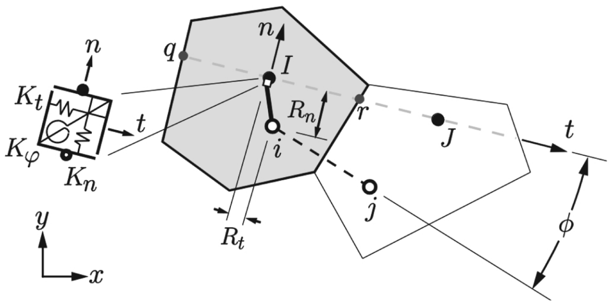

(b) Interfacial link element (2-D schematic)

Fig. 4 Modeling of concrete-reinforcement interface

$$A_{sc} = (1-\xi)A_s \tag{6}$$

where A_s is the original cross-section area of the bar and ξ is the relative weight loss due to corrosion

$$\xi = \frac{W_o - W_c}{W_o} \tag{7}$$

in which W_o is the initial weight of rebar and W_c is the weight of corroded rebar (after cleaning with a wire brush). Implicit within this calculation is the assumption that corrosion is practically uniform along the length of the bar. The properties of the reinforcement and bond link elements could reflect time-dependent deterioration according to models that account for the ingress and actions of aggressive agents (Biondini *et al.* 2006, Vořechovská *et al.* 2009). Based on such models, individual reinforcement or bond link elements could undergo differing degrees of deterioration.

2.3 Concrete-reinforcement interface

Each frame element node I is connected to the lattice node i associated with the same Voronoi cell. The connection is made via an ordinary bond link, similar to that of Ngo and Scordelis (1967),

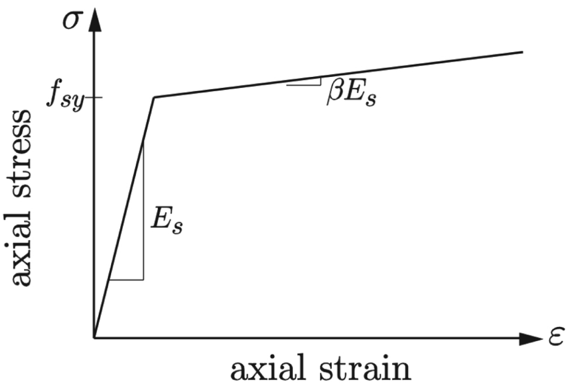

Fig. 5 Constitutive curve of reinforcing steel

and a rigid-body constraint, as shown in Fig. 4. These linkages are generated automatically, along with the frame elements. Similar automatic meshing capabilities, where the reinforcement nodes are freely positioned in the domain, have been developed within the context of 3-D finite element analysis of reinforced concrete (Barzegar and Maddipudi 1994, 1997). For the three-dimensional case, the axial and rotational spring coefficients for the bond link are

$$\mathbf{D}_L = \mathrm{diag}[K_t, K_m, K_n, K_{\phi t}, K_{\phi m}, K_{\phi n}] \tag{8}$$

from which the link element stiffness matrix is constructed

$$\mathbf{k}_L = \mathbf{T}^T(\mathbf{B}_L^T\mathbf{D}_L\mathbf{B}_L)\mathbf{T} \tag{9}$$

where $\mathbf{B}_L$ is the matrix relating generalized nodal (iI) displacements to the generalized displacements acting across the zero-size bond link

$$\mathbf{B}_L = [\mathbf{B}_1 \;\; \mathbf{I}] \tag{10}$$

and

$$\mathbf{B}_1 = \begin{bmatrix} -1 & 0 & 0 & 0 & -R_n & R_m \\ & -1 & 0 & R_n & 0 & -R_t \\ & & -1 & -R_m & R_t & 0 \\ & & & -1 & 0 & 0 \\ & & & & -1 & 0 \\ & & & & & -1 \end{bmatrix} \tag{11}$$

The offsets R_t and R_n are shown in Fig. 4 for the two-dimensional case.

The one of the axial springs of the link is aligned with the direction of the frame element. The stiffness of this spring, K_t, represents the nonlinear stress-slip property of the interface. This is prescribed by a piecewise linear function defined by N control points (Fig. 6), where s and τ

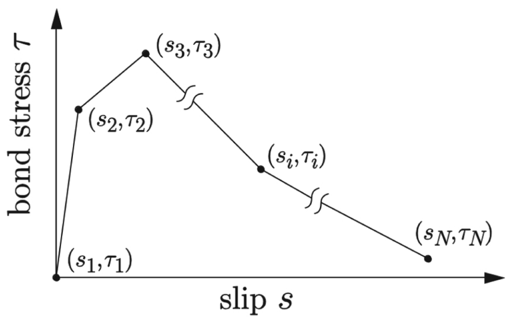

Fig. 6 Piecewise linear representation of bond stress-slip properties

represent bond slip and stress, respectively. The tributary bond length assigned to the link element *iI* is equal to the length of the corresponding segment of reinforcement traversing Voronoi cell *i*, i.e., the length of $\overline{qr}$ in Fig. 4(b).

In formulating the stiffness matrix of the frame elements representing the reinforcement, the axial stiffness coefficient of element *IJ* is multiplied by

$$\varsigma = \frac{h_{ij}\cos\phi}{h_{IJ}} \tag{12}$$

in which h_{IJ} is the element length and ϕ is the angle between the direction of frame element *IJ* and that of the corresponding lattice element *ij* (Fig. 4(b)). The need for this adjustment is apparent when considering uniform straining of the concrete material in the direction of the reinforcement. The rigid-body constraints (that are part of the bond-link element formulation) would impose non-uniform straining along the length of the reinforcement. The introduction of ς corrects this problem, so that the reinforcing bar also strains uniformly for that fundamental loading condition.

The line element discretization of the reinforcement, and the fairly coarse discretization of the surrounding concrete, precludes micromechanical modeling of corrosion induced cracking and its effects on bond between the reinforcement and concrete. Grassl and Davies (2011) and Tran *et al.* (2011) discretize the reinforcing bar volume and simulate corrosion induced cracking of the surrounding concrete. However, such models are computationally expensive. The use of line elements is more amenable to larger-scale analyses of RC structures, in which there is normally a multitude of bars.

2.4 Solution strategy

A classical lattice approach is used to model concrete cracking, i.e., a single-event driven solution scheme is used. The most critical element in the network is identified by a criticality factor $\kappa = \max(\sigma_i/f_t)$ for all elements *i*. In contrast to classical lattice approaches, where the most critical element (with $\kappa \geq 1$) is removed from the network, the breaking process is gradual and follows the softening relation shown in Fig. 3(b). The implementation of material softening is similar to the sequentially linear (saw-tooth) approach of Rots *et al.* (2008).

Since a maximum of one element breaks per computation cycle, iterative solution schemes are attractive. For larger systems, direct solution methods (such as those based on a factorization of **K** via Gaussian elimination) are problematic due to the need to reconstruct and factorize the system stiffness matrix with each element breakage. For the simulations of concrete fracture presented in this paper, the Cholesky decomposition $\mathbf{K} = \mathbf{L}\mathbf{L}^T$ is performed once (for the first load step) and later modified according to

$$\mathbf{L}^{i+1}(\mathbf{L}^{i+1})^T = \mathbf{L}^i(\mathbf{L}^i)^T - \mathbf{W}_j(\mathbf{W}_j)^T \tag{13}$$

where $\mathbf{W}_j(\mathbf{W}_j)^T$ is the reduction in stiffness of element j due to fracture event i, and

$$\mathbf{W}_j = (\mathbf{T}^T\mathbf{B}^T\sqrt{\Delta\mathbf{D}})_j \tag{14}$$

Large savings in computation effort are realized by this low-rank update of the Cholesky factorization, in which $\mathbf{L}^{i+1}$ is obtained directly from $\mathbf{L}^i$ and $\mathbf{W}_j$ (Davis and Hager 2001, Gill *et al.* 1974, Nukala *et al.* 2005, Yip *et al.* 2005). The nonlinear solution process then requires only a triangular solve operation using $\mathbf{L}^{i+1}$ for each element breakage. The implementation of the low-rank updates is done in conjunction with a compacted column (skyline) storage scheme and Crout factorization (Hughes 1987).

The same approach could be extended to handling nonlinear behavior for the other element types, i.e., low-rank updating of the most critical frame and link elements for each computational cycle. The process would be similar to that used for the concrete elements in that the **D** matrix for all elements considered here is diagonal and of rank six. As an intermediate approach, the complete reconstruction/factorization is done every p cycles to catch the state changes of the frame and link element types. This is effective, in part, due to the much greater number of concrete elements. For the RC beam analyses presented later, the period was set to $p = 20$.

3. Calibration of bond stress-slip relations

Control points for the bond stress-slip curve of an interfacial link element can be calibrated through comparisons with data obtained from bar pullout tests. Ideally, calibrations would utilize a large database of experimental results, covering various test configurations and bond conditions (Bhargava *et al.* 2008). In this paper, the experimental results of Al-Sulaimani *et al.* (1990) are used to assign bond stress-slip properties of the link elements for varying degrees of corrosion. The bond stress-slip properties are used for the analyses of RC beams in section 4.

For the bar pullout tests, Al-Sulaimani *et al.* (1990) used 10, 14, and 20 mm diameter bars centrally embedded within 150 mm concrete cubes, as shown in Fig. 7. The compressive strength of concrete used for these tests was $f_c = 30$ MPa. The short bonded length (of four times the bar diameter) was used to preclude other forms of failure, such as radial splitting of the concrete or steel yield. Pullout tests for the 14 mm bars, considered here, were conducted for varying degrees of corrosion ranging from $\xi = 0$ to 6.50%. Average bond stress is calculated by dividing external load on the rebar by circumferential area of the embedded portion.

The ascending branch of the stress-slip curves was modeled by

$$\tau(s) = \tau_0\left(\frac{s}{s_0}\right)^{\lambda} \tag{15}$$

where τ_0 and s_0 are the peak bond stress and corresponding slip, respectively. Two settings of λ

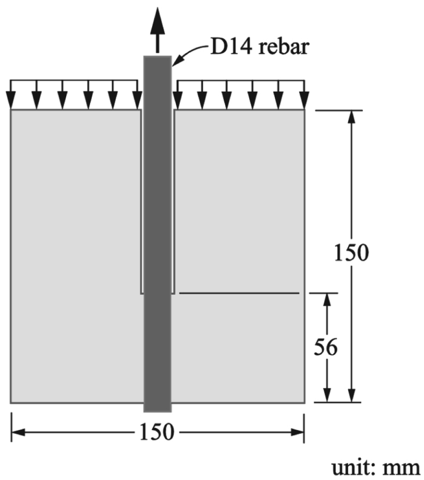

Fig. 7 Cross-section view of pull-out test configuration

Table 1 Estimation of concrete properties by empirical formulae (Mehta and Monteiro 1993, Nawy 2003)

Material property	Relation with the compressive strength
Tensile strength	$f_t = 0.324(f_c)^{2/3}$ (MPa)
Elastic modulus	$E_c = 4730\sqrt{f_c}$ (MPa)
Fracture energy	$G_F = 30(f_{cm}/10)^{0.7}$ (N/m)

Note: f_{cm} is the average 28-day compressive strength which can be replaced by $f_c + 8$ (MPa).

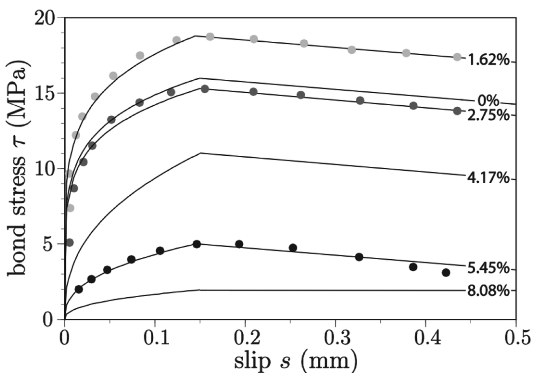

Fig. 8 Bond stress-slip experimental data points (for 14 mm bars of Al-Sulaimani *et al.* (1990)) and model curves for several degrees of bar corrosion

were used to fit the experimental data: λ = 0.18 for the lower corrosion levels for which no cracking was observed prior to testing; and λ = 0.4 for corrosion levels of 2.75% and beyond, for which specimens exhibited cracking prior to loading (Al-Sulaimani *et al.* 1990). In Fig. 8, bond stress-slip curves are fitted to the available data points for three levels of corrosion. For the lower (1.62%) corrosion levels, the bond properties improve, as has been noted in other studies (Al-

Sulaimani *et al.* 1990, Bhargava *et al.* 2008, Chung *et al.* 2008). The additional curves shown in Fig. 8 are for the beam analyses that follow. According to Eq. (15) the initial bond stiffness is infinite, so that a secant branch is used in the numerical implementation of the bond curves.

This form of calibration does not take into account coupling between mechanical behavior (such as cracking) and corrosion processes that can occur in actual structures. More sophisticated calibration procedures, or representation of the time-variant degradation processes (Biondini *et al.* 2006, Vořechovská *et al.* 2009), are needed to simulate such coupling.

4. Analyses of beams with corroded reinforcement

Using the bond properties determined through calibration, flexural tests of RC beams are simulated and compared with the corresponding experiments of Lee (1997). The beam dimensions and boundary conditions, as well as the positioning of longitudinal reinforcement (13 mm diameter bars) and stirrups (6 mm diameter bars), are shown in Fig. 9(a). The beams are under-reinforced and designed to fail in a flexural mode. During lattice model construction, only half of the specimen is modeled and symmetry boundary conditions are applied to nodes alongside the plane of symmetry (Fig. 9(b)). Both the longitudinal rebars and stirrups, and their linkages to the surrounding concrete elements, are discretely modeled as described in sections 2.2 and 2.3. Three corrosion degrees are considered, corresponding to three stages of corrosion in the otherwise nominally

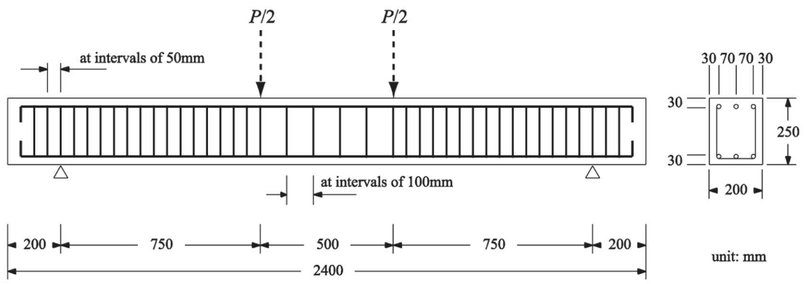

(a) Test specimen configuration

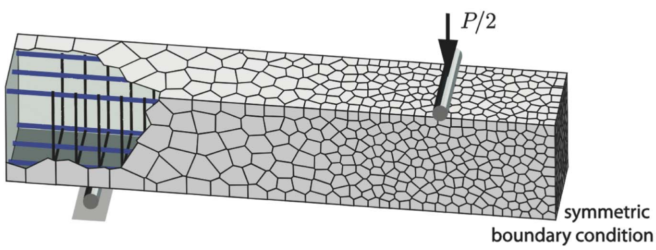

(b) Surface discretization and partial view of reinforcement elements in modeling of test specimen

Fig. 9 Flexural test configuration and model layout

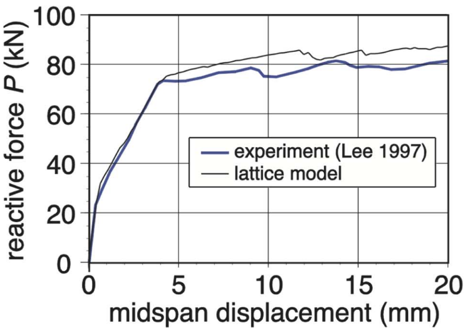

(a) specimen C-0

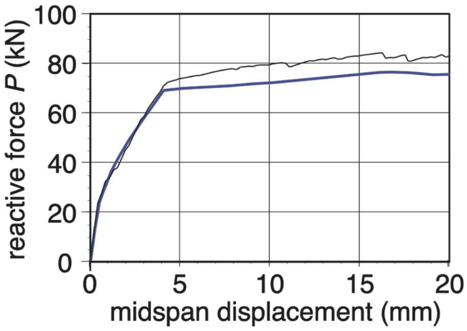

(b) specimen C-4

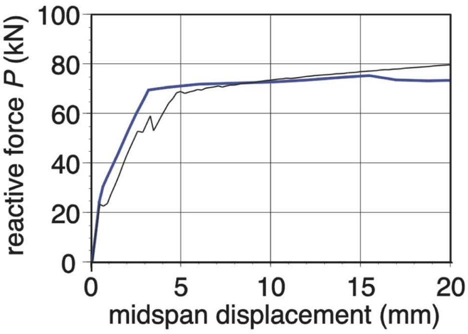

(c) specimen C-8

Fig. 10 Comparisons of load-deflection response for varying degrees of corrosion

identical beam experiments: $\xi = 0.0$, 4.17, and 8.08%, which are average values measured for the longitudinal bars within the test program (Lee 1997). In the following discussions, these beam specimens are designated C-0, C-4 and C-8, respectively.

The experimental program provided compressive strength of concrete, $f_c = 33.4$ MPa, and the elastic modulus E_s and yield stress f_{sy} of the non-corroded rebar as 186 GPa and 343 MPa, respectively. Other properties needed for the simulations have been calculated by formulae given in Table 1; the softening diagram (presented in Fig. 3(b)) is defined by $\gamma = 0.25$ and $\eta = 0.1$, which reasonably represents behavior witnessed in concrete fracture testing (Rokugo 1989). The parameters settings within Eq. (15), defining the concrete-steel interface for the three corrosion cases (C-0, C-4, and C-8), are obtained by interpolating between (or extrapolating from) neighboring values provided in (Al-Sulaimani *et al.* 1990). For the case of specimen C-8, it is assumed that $\tau = \tau_0$ for $s \geq s_0$. The resulting bond stress curves are presented in Fig. 8. Bar cross-section area depends on the degree of corrosion, as given by Eq. (6). It is assumed that stirrups are not corroded in any case.

The load is applied incrementally by displacement control up to several times the displacement associated with yielding of the reinforcement. Fig. 10 compares the experimental and simulated load-deflection response curves for each degree of corrosion. The two sets of results agree well, particularly with respect to the loads of first cracking and yielding of the tensile reinforcement. When considering the different degrees of corrosion, the most obvious difference is the lowering of

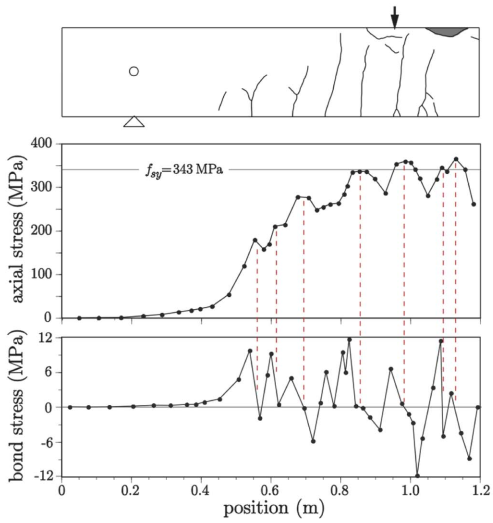

(a) specimen C-0

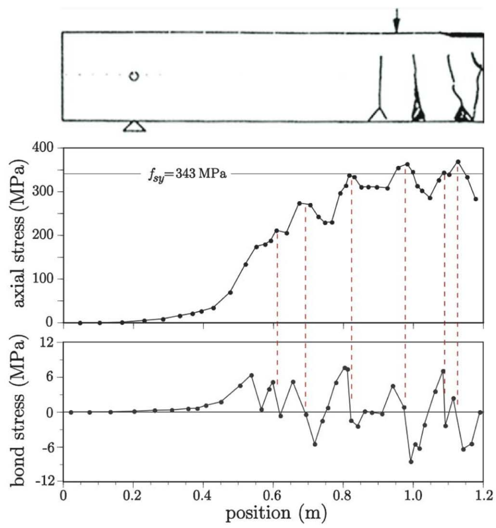

(b) specimen C-4

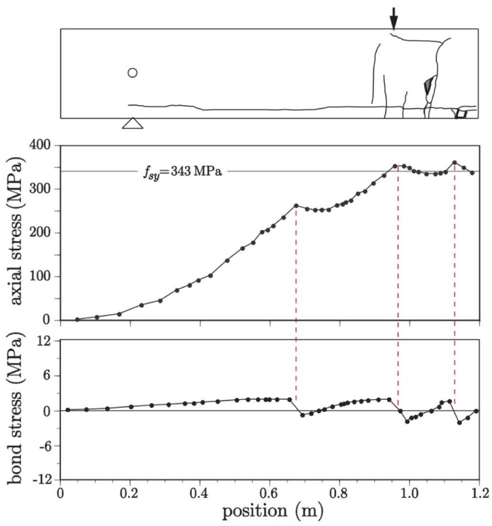

(c) specimen C-8

Fig. 11 Crack patterns (adapted from results of Lee (1997)), axial stress of tensile reinforcement, and bond stress distribution along tensile reinforcement for each beam specimen

the yield-point load with increasing corrosion. The load reduction is proportional to the loss of bar area due to corrosion. The immediate loss of load and stiffness due to crack formation are evident in the load-displacement response for the C-8 specimen, but not for the C-0 and C-4 specimens (Fig. 10). Apparently, the better bond of the non-corroded (and lowly corroded) bars helps control the rate of crack opening. Such effects of flexural cracking are not apparent in the experimental load-displacement curves, but that might be due to methods of load application and measurement.

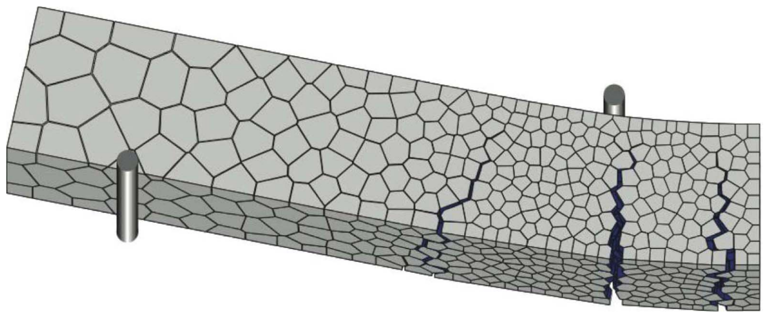

Fig. 12 Deformed mesh for 8% corrosion case (at midspan displacement of 10 mm)

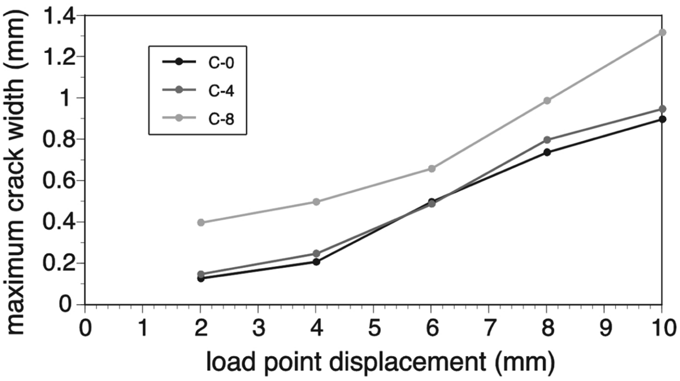

Fig. 13 Variation of maximum crack width with load-point displacement

Whereas the load-displacement responses are qualitatively similar for the corrosion degrees considered, the cracking modes are different. Fig. 11 presents cracking patterns recorded during the experiments for each corrosion degree, followed by plots of axial stress and bond stress along the central bar of the tensile reinforcement obtained from the lattice model. These numerical results correspond to a mid-span displacement of about twice the yield displacement (≈10 mm). For higher degrees of corrosion, bond stresses diminish and there is a tendency toward the formation of fewer, larger cracks. The locations of cracking in the model are indicated by local increases in bar axial stress and reversals in the sign of bond stress. Considering specimen C-8, for example, the three apparent locations of crack development in Fig. 11(c) correspond to instances of strain localization (displacement jumps) in the deformed lattice (Fig. 12). The C-0 and C-4 specimen models exhibit a similar correspondence between local increases in bar axial stress and crack patterns visible in the deformed lattice. Although crack widths were not reported for the experimental program, such information is provided by the numerical model. For the case of highly corroded bars, the maximum crack openings are significantly larger compared to cases with little or no corrosion (Fig. 13). The difference in crack openings is presented at the moment of first cracking and continues up beyond steel yield.

For the C-0 specimen, the number of cracks and the range of cracking over the half-span length agree fairly well with the cracking pattern recorded during the experiments. Reasonable agreement is seen for the C-8 specimen, in the sense that both the number of cracks and their range are reduced. In the experiment, however, the C-8 specimen exhibited a longitudinal crack along the length of the tensile reinforcement. The effects of such splitting cracking are indirectly represented by the form of the bond stress-slip relation (Fig. 8), since radial cracking occurred in the pullout tests of highly corroded bars used for calibration. Radial cracking, spalling, and delamination of the cover concrete are forms of damage caused by expansive corrosion of rebars (Allampallewar *et al.* 2008). Such forms of corrosion-induced damage could be explicitly simulated by a volumetric representation of rebars and the surrounding the concrete (Grassl and Davies 2011, Tran *et al.* 2011), although the modeling scale and objectives are typically limited by the increase in computational expense. With respect to specimen C-4, it is evident from the differences in cracking behavior that the bond strength and stiffness are over-estimated in the numerical model; more bond slip appears to have occurred in the experiment, thus causing fewer cracks. Some of these differences can be attributed to the large scatter reported in the literature for normalized bond strength as a function of corrosion degree (Bhargava *et al.* 2008). In addition, the confinement conditions in the pullout tests used for calibration differ from those of the beam tests.

5. Conclusions

This paper introduces an irregular lattice model of structural concrete, which is an extension of previous work (Yip *et al.* 2005) to account for nonlinear material behavior, including concrete cracking, reinforcing steel yield, and bond-slip along the concrete-steel interface. Lattice-type elements are used to represent the concrete, steel, and concrete-steel interface as distinct entities. The lattice model is applied to studying the effects of bond degradation due to corrosion on structural response. Flexural tests of Lee (1997) serve as a basis for comparison. The dependence of bond properties on corrosion was prescribed according to results from bond pullout specimens. Although the bond conditions for Lee's beam tests and the pullout tests are not equivalent, the calibration gives some indication of the relative changes in bond properties for different degrees of corrosion.

Numerical results compare favorably to experimental results with respect to load-displacement response and, to some degree, the cracking patterns. These results confirm several known observations, including:

1. The degrees of corrosion considered here, up to $\xi = 8\%$, affect the global load-displacement response mainly due to loss of bar cross-section area. Shifting of the yield load is in proportion to the area of cross-section lost due to corrosion.
2. Significant loss of bond translates into fewer, wider cracks. This holds true for the initial (pre-yield) cracking behavior, as well. For the simulations considered herein, the highly corroded member exhibits a threefold increase in maximum crack width in the pre-yield stages of the loading history, which are representative of the conditions expected under service loading.

Future work on this type of model should look at the sensitivity of bond modeling (e.g., the stress profiles in Fig. 11) to grid resolution local to the tensile reinforcement. The reinforcing bars themselves, including the bar lugs, could be discretized using the lattice elements for volumetric representation and that would be a natural means for including the coupling between bar slippage and radial stress production that potentially leads to radial splitting of the concrete, as seen for specimen C-8 in the experiment (Lee 1997). This would also enable the modeling of the various transport and electro-chemical processes contributing to steel corrosion, as well as the corresponding expansive pressures associated with iron oxide production. The likelihood or rate of steel corrosion are greatly increased by cracking of the concrete cover and recent developments of this lattice approach enable simulation of mass transport via discrete cracks, as a function of crack width (Grassl 2009, Nakamura *et al.* 2006). One main obstacle is the large computational costs associated with a sufficiently fine discretization of reinforced concrete structure.

With improvements in the physical bases of bond modeling, this lattice approach could be used as part of a performance based methodology for serviceability assessment of reinforced concrete affected by corrosion (Biondini *et al.* 2006, Li *et al.* 2005). Advantages are in ease of representing reinforcing elements irrespective of the discretization pattern used for the concrete, discrete-like modeling of bond and cracking, and stability of the computational approach.

Acknowledgements

This research was supported by a grant from the LNG Plant R&D Center funded by the Ministry of Land, Transportation and Maritime Affairs (MLTM) of the Korean government.

References

Abrishami, H.H. and Mitchell, D. (1992), "Simulation of uniform bond stress", *ACI Mater. J.*, **89**(2), 161-168.
Abrishami, H.H. and Mitchell, D. (1996), "Analysis of bond stress distributions in pullout specimens", *J. Struct. Eng.-ASCE*, **122**(3), 255-261.
Allampallewar, S.B. and Srividya, A. (2008), "Modeling cover cracking due to rebar corrosion in RC members", *Struct. Eng. Mech.*, **30**(6), 713-732.
Al-Sulaimani, G.J., Kaleemullah, M., Basunbul, I.A. and Rasheeduzzafar (1990), "Influence of corrosion and cracking on bond behavior and strength of reinforced concrete members", *ACI Struct. J.*, **87**(2), 220-231.
Barzegar, F. and Maddipudi, S. (1994), "Generating reinforcement in FE modeling of concrete structures", *J. Struct. Eng.-ASCE*, **120**(5), 1656-1662.
Barzegar, F. and Maddipudi, S. (1997), "Three-dimensional modeling of concrete structures. II: reinforced concrete", *J. Struct. Eng.-ASCE*, **123**(10), 1347-1356.
Bažant, Z. (1979), "Physical model for steel corrosion in concrete sea structures - theory", *J. Struct. Div.-ASCE*, **105**(6), 1137-1153.
Bažant, Z.P. and Oh, B. (1983), "Crack band theory for fracture of concrete", *RILEM Mater. Struct.*, **16**, 155-176.
Berton, S. and Bolander, J.E. (2006), "Crack band modeling of fracture in irregular lattices", *Comput. Method Appl. M.*, **195**, 7172-7181.
Bhargava, K., Ghosh, A.K., Mori, Y. and Ramanujam, S. (2008), "Suggested empirical models for corrosion-induced bond degradation in reinforced concrete", *J. Struct. Eng.-ASCE*, **134**(2), 221-230.
Biondini, F., Bontempi, F., Frangopol, D. and Malerba, P. (2006), "Probabilistic service life assessment and maintenance planning of concrete structures", *J. Struct. Eng.-ASCE*, **132**(5), 810-825.
Bolander, J.E., Hong, G.S. and Yoshitake, K. (2000), "Structural concrete analysis using rigid-body-spring networks", *Comput.-Aided Civ. Inf.*, **15**, 102-133.
Bolander, J.E. and Saito, S. (1998), "Fracture analyses using spring networks with random geometry", *Eng. Fract. Mech.*, **61**, 569-591.
Bolander, J.E. and Sukumar, N. (2005), "Irregular lattice model for quasistatic crack propagation", *Phys. Rev. B*, **71**(9), 094106.
Cairns, J. and Abdullah, R.B. (1996), "Bond strength of black and epoxy-coated reinforcement - a theoretical approach", *ACI Mater. J.*, **93**(4), 362-369.

Chung, L., Najm, H. and Balaguru, P. (2008), "Flexural behavior of concrete slabs with corroded bars", *Cement Concrete Comp.*, **30**(3), 184-193.

Ciampi, V., Eligehausen, R., Bertero, V.V. and Popov, E.P. (1982), *Analytical Model for Concrete Anchorages of Reinforcing Bars under Generalized Excitations*, Tech. Rep. 82/23, University of California, Berkeley.

Coronelli, D. (2002), "Corrosion cracking and bond strength modeling for corroded bars in reinforced concrete", *ACI Struct. J.*, **99**(3), 267-276.

Davis, T.A. and Hager, W.W. (2001), "Multiple-rank modifications of a sparse Cholesky factorization", *SIAM J. Matrix Anal. A.*, **22**(4), 997-1013.

Eligehausen, R., Popov, E.P. and Bertero, V.V. (1983), *Local Bond Stress-slip Relationships of Deformed Bars under Generalized Excitations*, Tech. Rep. 82/23, University of California, Berkeley.

Gill, P., Golub, G., Murray, W. and Saunders, M. (1974), "Methods for modifying matrix factorizations", *Math. Comput.*, **28**(126), 505-535.

Grassl, P. (2009), "A lattice approach to model flow in cracked concrete", *Cement Concrete Comp.*, **31**, 454-460.

Grassl, P. and Davies, T. (2011), "Lattice modelling of corrosion induced cracking and bond in reinforced concrete", *Cement Concrete Comp.*, **33**(9), 918-924.

Hansen, E. and Saouma, V. (1999), "Numerical simulation of reinforced concrete deterioration: Part II - steel corrosion and concrete cracking", *ACI Mater. J.*, **96**, 331-337.

Hughes, T. (1987), *The Finite Element Method - Linear Static and Dynamic Finite Element Analysis*, Prentice-Hall.

Kawai, T. (1978), "New discrete models and their application to seismic response analysis of structures", *Nucl. Eng. Des.*, **48**, 207-229.

Lee, H. (1997), "Evaluation of structural performance and strengthening of corrosion deteriorated reinforced concrete members", Ph.D. thesis, Tokyo University, Japan.

Li, C., Lawanwisut, W. and Zheng, J. (2005), "Time-dependent reliability method to assess the serviceability of corrosion-affected concrete structures", *J. Struct. Eng.-ASCE*, **131**(11), 1674-1680.

Liu, Y. and Weyers, R. (1998), "Modeling the time-to-corrosion cracking in chloride contaminated reinforced concrete structures", *ACI Mater. J.*, **95**(6), 675-681.

Mathey, R.G. and Watstein, D. (1961), "Investigation of bond in beam and pull-out specimens with high-yield-strength deformed bars", *J. Am. Concrete I.*, **57**, 1071-1090.

McGuire, W. and Gallagher, R.H. (1979), *Matrix Structural Analysis*, John Wiley and Sons.

Mehta, P.K. and Monteiro, P.J.M. (1993), *Concrete: Structure, Properties, and Materials*, Prentice Hall.

Nakamura, H., Srisoros, W., Yashiro, R. and Kunieda, M. (2006), "Time-dependent structural analysis considering mass transfer to evaluate deterioration process of RC structures", *J. Adv. Concr. Technol.*, **4**, 147-158.

Nawy, E.G. (2003), *Reinforced Concrete: A Fundamental Approach*, Prentice Hall.

Ngo, D. and Scordelis, A.C. (1967), "Finite element analysis of reinforced concrete beams", *J. Am. Concrete I.*, **64**(3), 152-163.

Nukala, P., Simunovic, S. and Guddati, M. (2005), "An efficient algorithm for modeling progressive damage accumulation in disordered materials", *Int. J. Numer. Meth. Eng.*, **62**(14), 1982-2008.

Pantazopoulou, S. and Papoulia, K. (2001), "Modeling cover-cracking due to reinforcement corrosion in RC structures", *J. Eng. Mech.*, **127**(4), 342-351.

Preparata, F.P. and Shamos, M.I. (1985), *Computational Geometry: An Introduction*, Springer-Verlag, New York.

Rokugo, K., Iwasa, M., Suzuki, T. and Koyanagi, W. (1989), "Testing method to determine tensile strain softening curve and fracture energy of concrete", *Fracture Toughness and Fracture Energy*, Balkema, 153-163.

Rots, J., Belletti, B. and Invernizzi, S. (2008), "Robust modeling of RC structures with an "event-by-event" strategy", *Eng. Fract. Mech.*, **75**, 590-614.

Stanish, K., Hooton, R.D. and Pantazopoulou, S.J. (1999), "Corrosion effects on bond strength in reinforced concrete", *ACI Struct. J.*, **96**(6), 915-921.

Sukumar, N. and Bolander, J.E. (2008), "Voronoi-based interpolants for fracture modelling", *Tessellations in the Sciences: Virtues, Techniques and Applications of Geometric Tilings*, Springer-Verlag, 1-27.

Tran, K.K., Nakamura, H., Kawamura, K. and Kunieda, M. (2011), "Analysis of crack propagation due to rebar corrosion using RBSM", *Cement Concrete Comp.*, **33**(9), 906-917.

Task Committee on Finite Element Analysis of Reinforced Concrete Structures (1982), *State-of-the-art Report on Finite Element Analysis of Reinforced Concrete*, Tech. Rep., ASCE.

Tuutti, K. (1982), *Corrosion of Steel in Concrete*, Swedish Cement and Concrete Research Institute.

Vořechovská, D., Podroužek, J., Chromá, M., Rovnaníková, P. and Teplý, B. (2009), "Modeling of chloride concentration effect on reinforcement corrosion", *Comput.-Aided Civ. Inf.*, **24**(6), 446-458.

Widom, B. (1966), "Random sequential addition of hard spheres to a volume", *J. Chem. Phys.*, **44**, 3888-3894.

Yip, M., Mohle, J. and Bolander, J.E. (2005), "Automated modeling of 3-D structural components using irregular lattices", *Comput.-Aided Civ. Inf.*, **20**(6), 393-407.